Available online at www.sciencedirect.com
ScienceDirect
Inorganica Chimica Acta 360 (2007) 329–344
Inorganica Chimica Acta
www.elsevier.com/locate/ica

Cycloaddition and electron transfer: On a synthetically useful aspect of pnictogen(I) reactivity

Bobby D. Ellis, Charles L.B. Macdonald *

Department of Chemistry and Biochemistry, University of Windsor, 401 Sunset Avenue, Windsor, Ont., Canada N9B 3P4

Received 5 July 2006; accepted 13 July 2006
Available online 28 July 2006

Inorganic Chemistry – The Next Generation.

Abstract

The behavior of several bi- or tri-dentate sp^2-nitrogen-containing ligands with phosphorus(I) and arsenic(I) centers is investigated using computational and, in some cases, experimental methods. Whereas the chelation of putative Pn^I cations (Pn = P, As) by 1,4-diazabutadienes (DAB) generate stable, isolable phosphenium or arsenium cations that contain Pn^{III} centers, the corresponding reactions of Pn^I cations with β-diketiminate (NACNAC) ligands do not yield similar planar heterocycles. The behaviors of the ligands 2,6-diiminopyridine and 2,2′-bipyridine fall between the extremes delimited by the DAB and NACNAC ligands. The results of computational investigations of potential products provide a framework to rationalize the chemistry observed.
© 2006 Elsevier B.V. All rights reserved.

Keywords: Low oxidation state; Group 15; Diimines; Diketiminates; Nitrogen ligands; Computational chemistry; Phosphenium; Arsenium; Charge transfer; Redox

1. Introduction

The oxidation state of an element in a molecule can have a significant influence on the structural features, bonding and chemistry of that molecule. In recent years, many main group chemists have been interested in the chemistry of compounds containing main group elements in unusually low oxidation states because such electron-rich species often exhibit behavior that is manifestly different than compounds containing the elements in more conventional oxidation states [1]. In regard to the heavier group 15 elements (pnictogens; Pn = P, As, Sb, Bi) we have been particularly interested in compounds containing the elements in the +1 oxidation state [2]. While phosphinidenes and their heavier Pn^I analogues, **1**, are generally highly reactive, transient species [3–5], in the 1980s, the seminal work of Schmidpeter demonstrated the viability of stable, di-coordinate cationic P^I compounds [6]. In particular, Schmidpeter's group showed that salts containing "triphosphenium" cations, **2**, which may be considered to consist of phosphine-stabilized P^I ions, can be obtained by the in situ reduction of PCl_3 in the presence of phosphine ligands, as depicted in Scheme 1. Some corresponding arsenic analogues have likewise been obtained using similar preparative approaches [7–11].

In the last five years, the research groups of Dillon and co-workers [12], Macdonald and co-workers [13–15] and Woollins and co-workers [16] have shown that it is possible to generate and isolate halide salts of triphosphenium ions and their arsenic analogues in the absence of additional reducing agents. When appropriate conditions are employed in reactions using chelating diphosphine ligands and PI_3, it has proven possible to obtain analytically pure iodide salts of the triphosphenium cations, as illustrated in Scheme 2. In a similar vein, it has been demonstrated that related P^I halide salts can be generated by the treat-

---

* Corresponding author. Tel.: +1 519 253 3000x3991; fax: +1 519 973 7098.
E-mail address: cmacd@uwindsor.ca (C.L.B. Macdonald).

0020-1693/$ - see front matter © 2006 Elsevier B.V. All rights reserved.
doi:10.1016/j.ica.2006.07.047

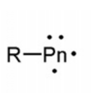

1

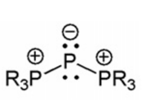

2

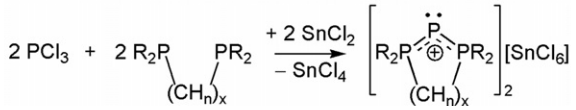

Scheme 1.

ment of PX_3 (X = Cl, Br, I) with certain *N*-heterocyclic carbenes, which exhibit comparable reactivity to phosphine ligands [17].

Recently, Cowley and co-workers have investigated the use of diimines as ligands for putative Pn^I cations generated by both of the synthetic protocols outlined above. In the case of a 1,2-bis(arylimino)acenapthene (Ar-BIAN), the reaction of $PnCl_3$ (Pn = P, As) and $SnCl_2$ in the presence of the BIAN ligand produced salts of the form [(Ar-BIAN)Pn][$SnCl_5 \cdot THF$] and the reactions of Ar-BIAN with PnI_3 generated the corresponding triiodide salts, [(Ar-BIAN)Pn][I_3]; these reactions are illustrated in Scheme 3 [18]. Regardless of the identity of the anion, the metrical parameters for the cations in these salts indicate that these cations are best described as phosphenium [19] or arsenium cations that contain Pn^{III} centers generated with the concomitant 2-electron reduction of the Ar-BIAN ligand. In this light, such products are analogous to those obtained when phosphinidene transfer agents are treated with α-diimines and related trapping agents [20]. Similar results are obtained from the analogous reactions of the simpler diimine 1,4-dimesityl-1,4-diazabutadiene (Mes-DAB) with AsI_3 or the $AsCl_3/SnCl_2$ mixture [21] and it is noteworthy that **3** was the perhaps surprising result from the reaction of R-DAB (*R* = Mes or ${}^tBu$) with PCl_3 and NEt_3 [22].

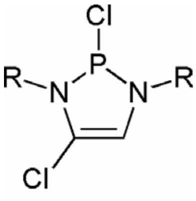

3

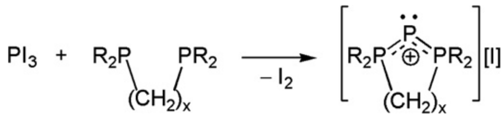

Scheme 2.

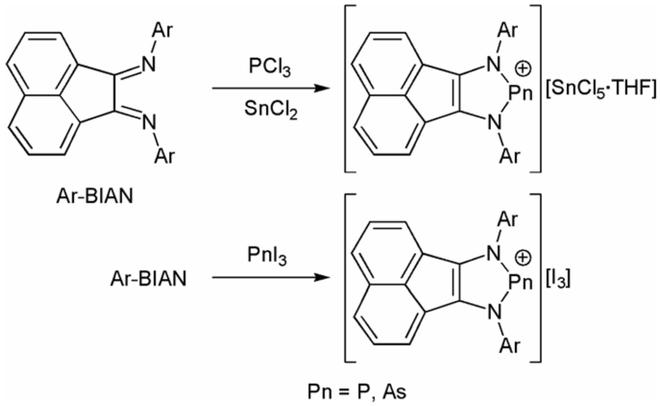

Scheme 3.

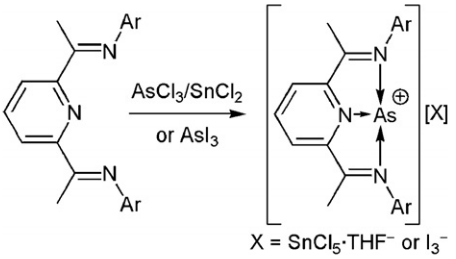

Scheme 4.

In contrast, the reaction of AsI_3 or $AsCl_3/SnCl_2$ with an α,α′-diiminopyridine (Ar-DIMPY, Scheme 4) ligand generates salts containing the cation $[(Ar\text{-}DIMPY)As]^+$; the metrical parameters in this cation are much more consistent with the presence of an As^I cation chelated by a non-reduced Ar-DIMPY ligand. The overall T-shaped arrangement about the As center is reminiscent of the so-called "10-As-3" center in Arduengo's unique family of group 15 compounds (**4**, Pn = P, As, Sb; *R* = ${}^tBu$ or adamantyl) containing the diketoamido ligand [23,24].

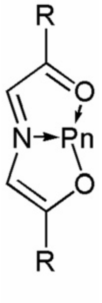

4

Given the importance of β-diketiminate (NACNAC) ligands to transition metal [25] and main group chemistry [26–28], several groups have attempted to coordinate such ligands to phosphorus centers. In stark contrast to the results outlined above for α-diimines, the reactions of metallated NACNAC reagents with halogenated P^{III} species results in the formation of a P–C bond to the unique

C_α atom instead of chelation by the nitrogen atoms [29–31]. The adoption of the monodentate binding mode and avoidance of P–N bond formation is also observed when reaction conditions are used that are analogous to those that have been employed successfully for the heterocycle syntheses described above.

In light of the range of products observed from seemingly similar reactions, herein we present computational and some experimental results that elucidate important aspects of the interactions between several chelates that contain sp^2-hybridized nitrogen centers and P^I and As^I centers. It is anticipated that the insight afforded by such investigations may facilitate the design of heterocycle forming reactions involving low oxidation state reagents.

2. Experimental

2.1. General methods

All work was carried out using standard inert-atmosphere techniques. Phosphorus(III) chloride, phosphorus(III) iodide, and tin(II) chloride were obtained from Strem; all solvents were obtained from Aldrich: all reagents were used without further purification. The preparations of 1,4-diaryl-2,3-dimethyl-1,4-diazabutadiene (ArM-DAB) [32] and Ar-NACNAC [33] (Ar = 2,6-diisopropylphenyl) are described in the literature. Solvents were dried on a series of Grubbs'-type columns [34] and were degassed prior to use. NMR spectra were recorded at room temperature in CD_2Cl_2 solutions on a Bruker Advance 300 MHz spectrometer. Chemical shifts are reported in ppm, relative to external standards ($SiMe_4$ for ^1H and ^{13}C, 85% aq. H_3PO_4 for ^{31}P). Coupling constants are given in Hertz. Melting points were obtained on samples sealed in glass capillaries under dry nitrogen using an Electrothermal® Melting Point Apparatus. Elemental analysis was performed using a Perkin–Elmer 2400 C, H, N analyzer in the Centre for Catalysis and Materials Research, Department of Chemistry and Biochemistry, University of Windsor. It should also be noted that the reactions appear to be quantitative according to all spectroscopic data recorded.

2.2. Preparation of $[(ArM\text{-}DAB)P][SnCl_5]$, **5**$[SnCl_5]$

Solid ArM-DAB (0.433 g; 1.070 mmol) was added to a $SnCl_2$ (0.203 g; 1.070 mmol) slurry in CH_2Cl_2 (20 mL), to afford a yellow slurry. A solution of PCl_3 (0.147 g; 1.070 mmol) in CH_2Cl_2 (10 mL) was slowly added and the mixture became red. The mixture was left to stir for 16 h and then it was filtered through Celite and the volatile components were removed in vacuo. Dissolution of the red solid in a minimal amount of CH_2Cl_2 followed by slow evaporation produced pink crystalline material. Yield: 88% (0.692 g; 0.946 mmol). $^{31}P\{^1H\}$ NMR: 200.7 (s). $^{13}C\{^1H\}$ NMR: 13.5 (s), 23.2 (s), 26.1(s), 29.4(s), 124.9(s), 125.8(s), 132.9(s), 144.3(s), 145.5(s). ^1H NMR: 1.21 (d, $J = 6.9$, 24H), 2.31 (s, 6H), 2.67 (septet, $J = 6.9$, 2H), 7.49 (d, $J = 7.8$, 4H), 7.69 (t, $J = 7.8$, 2H). m.p.: 215–216 °C. *Anal.* Calc. for $C_{28}H_{40}Cl_5N_2PSn$ (731.578): C, 45.97; H, 5.51. Found: C, 45.78; H, 5.45%.

2.3. Preparation of $[(ArM\text{-}DAB)P][I_3]$, **5**$[I_3]$

Solid ArM-DAB (0.352 g; 0.870 mmol) was added to a solution of PI_3 (0.358 g; 0.870 mmol) in CH_2Cl_2 (15 mL), which immediately changed from reddish-orange to dark red. The solution was left to stir for 16 h and then the volatile components were removed in vacuo. Dissolution of the red solid in a minimal amount of MeCN followed by slow evaporation produced red crystalline material. Yield: 84% (0.597 g; 0.731 mmol). $^{31}P\{^1H\}$ NMR: 201.1 (s). $^{13}C\{^1H\}$ NMR: 13.9(s), 23.3 (s), 26.1(s), 29.5 (s), 125.0 (s), 125.8 (s), 132.9 (s), 144.3 (s), 145.5 (s). ^1H NMR: 1.22 (d, $J = 7.0$, 24H), 2.31 (s, 6H), 2.67 (septet, $J = 7.0$, 2H), 7.48 (d, $J = 7.9$, 4H), 7.67 (t, $J = 7.9$, 2H). m.p.: 290–291 °C. *Anal.* Calc. for $C_{28}H_{40}I_3N_2P$ (816.318): C, 41.20; H, 4.94. Found: C, 41.47; H, 4.93%.

2.4. X-ray crystallography

Each crystal was covered in Nujol and placed rapidly into the cold N_2 stream of the Kryo-Flex low temperature device. The data were collected using the SMART [35] software on a Bruker APEX CCD diffractometer using a graphite monochromator with Mo Kα radiation ($\lambda = 0.71073$ Å). A hemisphere of data were collected using a counting time of 30 s per frame. The data were collected at −100 °C. Details of crystal data, data collection and structure refinement are listed in Table 1. Data reductions were performed using the SAINT [36] software and the data were corrected for absorption using SADABS [37]. The structures were solved by direct methods using SIR-97 [38] and refined by full-matrix least-squares on F^2 with anisotropic displacement parameters for the non-H atoms using SHELXL-97 [39] and the WinGX [40] software package and thermal ellipsoid plots were produced using SHELXTL [41].

2.5. Theoretical methods

Calculations were preformed with the GAUSSIAN-98 suite of programs [42]. Geometry optimizations have been calculated using density functional theory (DFT), specifically implementing the B3PW91 method [containing Becke's three-parameter hybrid functional for exchange (B3, including ca. 20% Hartree–Fock exchange) [43] combined with the generalized gradient approximation for correlation of Perdew and Wang (PW91) [44]] in conjunction with the 6-31+G(d) basis set. The geometries were restricted to the highest appropriate symmetry and the nature of each stationary point was examined by vibrational frequency analysis; in certain instances, the data obtained for the C_{2v}-symmetry structures, which are identified as transition states, are reported because they provide the most appro-

Table 1
Summary of X-ray crystallographic data for compounds **5**[SnCl$_5$] and **5**[I$_3$]

Compound	**5**[SnCl$_5$]	**5**[I$_3$]
Empirical formula	$C_{28}H_{40}Cl_5N_2PSn$	$C_{28}H_{40}I_3N_2P$
Formula weight	731.53	816.29
Temperature (K)	173(2)	173(2)
Wavelength (Å)	0.71073	0.71073
Habit, color	prism, pink	prism, red
Crystal system	orthorhombic	monoclinic
Space group	*Pnma*	*C*2/*m*
Unit cell dimensions		
a (Å)	20.805(3)	19.044(2)
b (Å)	15.709(2)	16.745(2)
c (Å)	10.7872(14)	11.6861(14)
α (°)	90	90
β (°)	90	120.005(1)
γ (°)	90	90
V (Å^3)	3525.6(8)	3227.2(7)
Z	4	4
D_{calc} (g cm^{-3})	1.378	1.680
Absorption coefficient (mm^{-1})	1.168	2.973
F(000)	1488	1584
θ Range for data collection (°)	2.13–27.50	1.73–27.50
Limiting indices	$-26 \leqslant h \leqslant 26$, $-20 \leqslant k \leqslant 19$, $-14 \leqslant l \leqslant 13$	$-24 \leqslant h \leqslant 24$, $-21 \leqslant k \leqslant 21$, $-15 \leqslant l \leqslant 15$
Reflections collected	37062	18204
Independent reflections (R_{int})	4178 (0.0492)	3798 (0.0235)
Absorption correction	SADABS	SADABS
Refinement method	full matrix least squares on F^2	full matrix least squares on F^2
Data/restraints/parameters	4178/0/185	3798/0/167
Goodness-of-fit on F^2	1.202	1.032
Final R indices[a] [$I > 2\sigma(I)$]	$R_1 = 0.0421$, $wR_2 = 0.0884$	$R_1 = 0.0418$, $wR_2 = 0.0944$
R indices (all data)	$R_1 = 0.0712$, $wR_2 = 0.1061$	$R_1 = 0.0539$, $wR_2 = 0.1027$
Largest difference map peak and hole (e Å^{-3})	1.277 and −0.487	1.466 and −1.532

[a] $R_1(F) = \sum(|F_o| - |F_c|)/\sum|F_o|$ for reflections with $F_o > 4(\sigma(F_o))$. $wR_2(F^2) = \{\sum w(|F_o^2| - F_c^2|)^2/\sum w(|F_o^2|)^2\}^{1/2}$ where w is the weight given each reflection.

priate models for structural and electronic structure comparisons. The electronic energies of the molecules have been corrected by the unscaled, zero-point vibrational energy (ZPVE). Single-point energies have been calculated at the B3PW91/6-311+G(3df,2p)//B3PW91/6-31G(d) level of theory. Population analyses were conducted using the natural bond orbital (NBO) [45] method implemented in GAUSSIAN-98. Drawings of the optimized structures of the model compounds were made using SHELXTL and depictions of the molecular orbitals were made using MOLDEN [46].

3. Results and discussion

3.1. Experimental investigations

Cowley recently demonstrated the differing behavior of some diimine-based ligands with P^{I} and As^{I} centers. In particular, whereas the α-diimines in Ar-BIAN or Mes-DAB formed phosphenium or arsenium cations that are best described as containing Pn^{III} centers, the analogous reactions with the 2,6-diimino substituted pyridine ligand appears to contain arsenic(I) centers. Given our interest in the chemistry of and the factors affecting the stabilization of low oxidation state main group fragments, these results prompted us to elucidate the nature of the interaction between the diimine ligands and the Pn^{I} centers and to assess the viability of some other commonly used ligands bearing imine-like moieties that contain sp^2-hybridized nitrogen centers.

In light of the apparently odd results observed when the β-dimine NACNAC ligands have been ligated to phosphorus centers [29–31], we wished to ascertain whether such diimines were suitable ligands for P^{I} centers, however, given the reported reactivity with halophosphines, a minor modification of the SnCl$_2$ reduction protocol was mandated [47]. In this vein, a solution of [Li][Ar-NACNAC] was added to an equimolar amount of SnCl$_2$ in THF to produce a cloudy, colorless mixture. After stirring for several minutes, a solution of an equimolar amount of PCl$_3$ in THF was added to the reaction mixture. The mixture rapidly produced a pale yellow precipitate and a yellow solution. The supernatant contained no signals in the ^{31}P NMR spectrum. Similarly, the reaction of [Li][Ar-NACNAC] with PI$_3$ in THF resulted in the immediate formation of a reddish solution and the formation of a copious amount of orange precipitate. The solution contains no signals in the ^{31}P NMR spectrum consistent with a neutral compound of the form [(Ar-NACNAC)P]. Likewise, the reaction of an equimolar mixture of [Ar-NACNAC]H and SnCl$_2$ in dichloromethane with a solution of PCl$_3$ in the same solvent produced a multitude of products. In each case, the reactions appeared to produce numerous products that have as yet eluded separation and identification, however, there is no evidence for the formation of a neutral compound of the form [(Ar-NACNAC)P]; these reactions are certainly not clean or quantitative.

To confirm that our modified synthetic approach was applicable for the preparation of P^{I} centers, similar reactions were undertaken with the α-diimine 1,4-diaryl-2,3-dimethyl-1,4-diazabutadiene (ArM-DAB). Thus an equimolar mixture of ArM-DAB and SnCl$_2$ in dichloromethane was stirred for several minutes and then a solution containing an equimolar amount of PCl$_3$ was added to produce a red solution. Multinuclear ^{1}H and ^{13}C NMR experiments on the reaction mixture indicated the presence of a singular, intact ArM-DAB ligand and the single peak at 200.1 ppm in the ^{31}P NMR spectrum suggested the quantitative formation of the phosphenium cation [(ArM-DAB)P]$^+$ (**5**). A crystalline solid was obtained by the slow concentration of a dichloromethane solution of the resultant solid and microanalysis was consistent with a salt of the form **5**[SnCl$_5$].

In a similar manner, the reaction of equimolar quantities of ArM-DAB and PI$_3$ in dichloromethane rapidly generates a red solution. Again, multinuclear NMR experiments of the reaction mixture attest to the presence of a singular, intact ArM-DAB ligand and the ^{31}P NMR spectrum contains only a single peak at 201.1 ppm. The slow concentration of an acetonitrile solution of the solid provided crystalline material having an elemental composition consistent with the formula **5**[I$_3$].

In the case of each salt, the material obtained after recrystallization was suitable for analysis by single-crystal X-ray diffraction experiments. A summary of the experimental crystallographic details are compiled in Table 1; depictions of the molecular structures of both salts are presented in Figs. 1 and 2; and selected metrical parameters for the salts are listed in the captions of each figure. The pentachlorostannate salt **5**[SnCl$_5$] crystallizes in the space group *Pnma* with one half of a cation and an anion in the asymmetric unit. The phosphorus atom sits on a crystallographic mirror plane that relates the two halves of the cation and the tin atom and three of the chlorine atoms are likewise situated on the mirror plane relating the two parts of the anion. The triiodide salt **5**[I$_3$] crystallizes in the spacegroup *C*2/*m* with one half of a cation and two quarters of anions in each asymmetric unit. Again, the phosphorus atom resides on a crystallographic mirror plane that relates the two halves of the cation and all of the iodine atoms are located on special positions in the unit cell.

While the metrical parameters of each of the anions in these salts compare well with the average values obtained from the Cambridge Structural Database (CSD) [48] and do not warrant further discussion, the identities of the anions unambiguously demonstrate that a redox reaction has taken place: the Sn^{II} in the starting material has clearly been oxidized to Sn^{IV} in the trigonal bipyramidal [SnCl$_5$]$^-$ anion and the production of triiodide anions is consistent with the presence of I$_2$ and I$^-$ in the other reaction mixture. It should be noted that there are no unusually short distances between the cations and the anions in either salt. For the purposes of this work, the metrical parameters of the cations in each salt are important for comparison to the computed structures detailed below and can aid in the assessment of the nature of the interaction between the diimine ligand and the pnictogen center. Regardless of the identity of the anion, the metrical parameters of the cation are indistinguishable. For example the P–N distance in **5**[SnCl$_5$] is 1.667(3) Å and the distance in the triiodide salt is 1.668(3) Å; similarly, the C–N and C–C distances within the heterocycle are 1.377(4) Å and 1.373(6) Å, respectively, in **5**[SnCl$_5$] versus 1.375(4) Å and 1.376(7) Å for **5**[I$_3$]. The corresponding angles within the heterocyclic cations in each salt are also indistinguishable from each other: the N–P–N angles are 88.88(17)° and 88.90(19)° in **5**[SnCl$_5$] and **5**[I$_3$], respectively; the P–N–C angles are 115.1(2)° and 115.1(2)°, respectively; and the N–C–C angles are 110.43(16)° and 110.43(18)°, respectively. Overall, the metrical parameters of the cations in these salts compare excellently with the average values obtained from the CSD for the other unsaturated five-membered ring phosphenium cations that have been

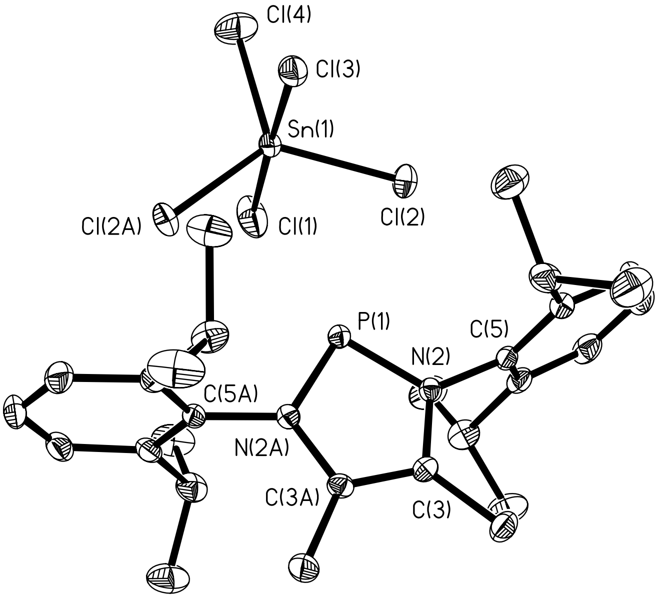

Fig. 1. Thermal ellipsoid plot (30% probability surfaces) of [(ArM-DAB)P][SnCl$_5$]. Hydrogen atoms are omitted for clarity. Selected distances (Å) and angles (°): P(1)–N(2) 1.667(3), N(2)–C(3) 1.377(4), C(3)–C(3A) 1.373(6), N(2)–C(5) 1.449(4), Sn(1)–Cl(1) 2.3782(16), Sn(1)–Cl(3) 2.4093(14), Sn(1)–Cl(2) 2.3411(9), Sn(1)–Cl(4) 2.3278(16), N(2)–P(1)–N(2A) 88.88(17), C(3)–N(2)–P(1) 115.1(2), C(3A)–C(3)–N(2) 110.43(16), Cl(2)–Sn(1)–Cl(1) 90.05(4), Cl(4)–Sn(1)–Cl(3) 91.31(6), Cl(1)–Sn(1)–Cl(3) 176.36(7), Cl(2)–Sn(1)–Cl(3) 88.25(3), Cl(4)–Sn(1)–Cl(3) 91.31(6), Cl(4)–Sn(1)–Cl(2) 117.92(3), Cl(2)–Sn(1)–Cl(2A) 124.11(5).

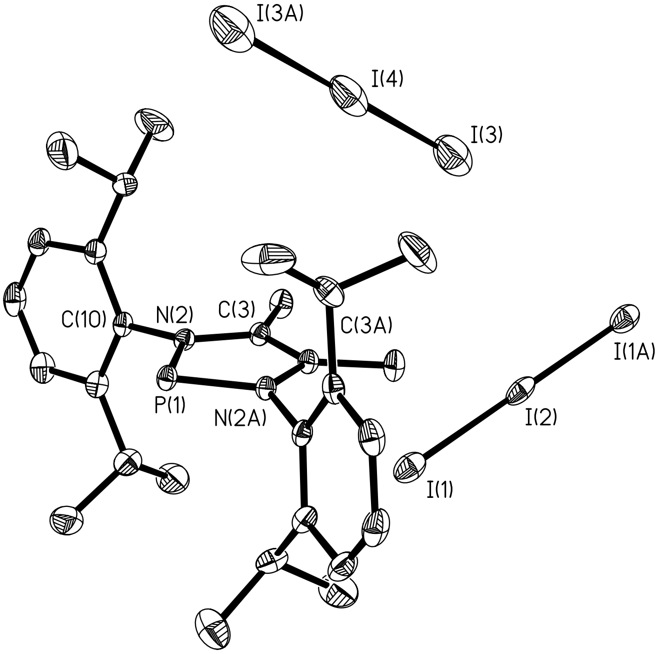

Fig. 2. Thermal ellipsoid plot (30% probability surface) of [(ArM-DAB)P][I$_3$]. Hydrogen atoms are omitted for clarity. Selected distances (Å) and angles (°): P(1)–N(2) 1.668(3), C(3)–N(2) 1.375(4), C(3)–C(3A) 1.376(7), N(2)–C(10) 1.456(4), I(2)–I(1) 2.9207(7), I(3)–I(4) 2.9435(9), N(2)–P(1)–N(2A) 88.90(19), C(3)–N(2)–P(1) 115.1(2), N(2)–C(3)–C(3A) 110.43(18), I(1)–I(2)–I(1A) 180.000(19), I(3)–I(4)–I(3A) 180.0.

reported previously [22,49–51], thus the descriptions of these cations as containing phosphorus(III) is certainly justified.

The nature of the anions in the phosphenium salts described above and the other salts described in the introduction indicates that redox processes occur in the formation of the heterocycles that are completely consistent with the processes postulated to occur in the formation of phosphine- or carbene-stabilized Pn^{I} salts [8,12,13,15,17]. In the case of α-diimines, a further intermolecular redox process involving oxidation of Pn^{I} to Pn^{III} and reduction of the ligand to its doubly-reduced form has been suggested to generate the observed pnictogenium cations [18,21]. In the case of the diimino-pyridine ligand, while the first redox reaction generates an As^{I} center and the corresponding anions, the intermolecular redox process does not appear to occur [21]. Finally, the β-diketiminate ligand does not appear to chelate to putative Pn^{I} centers under conditions analogous to those employed for the other imine-containing ligands [47].

3.2. Computational investigations

In an attempt to understand the clearly different chelating behavior of the various diimine ligands and Pn^{I} centers, we performed a series of DFT calculations and NBO analyses on the model compounds of the Pn-containing compounds chelated by the ligands DAB, NACNAC, DIMPY and BIPY. Models of the free ligands and their doubly-reduced forms are also presented for comparative purposes. Additional calculations were undertaken on the dications $[(NACNAC)Pn]^{2+}$ to assess the viability of β-diketiminate chelate of Pn^{III} cations. In each model, all substituents have been replaced with hydrogen atoms and the highest-reasonable point symmetry was enforced; important computational results are compiled in Table 2 and more complete data are found in the Supporting information.

The C_{2v}-symmetry optimized geometries of the phosphorus- and arsenic-containing model compounds are depicted in Figs. 3 and 4, respectively, and the computed values of important metrical parameters are provided. The only phosphorus compound for which analogues have been structurally characterized experimentally (with substituents other than hydrogen) is the cation $[(DAB)P]^{+}$; given the simplicity of the model used, the agreement between the metrical parameters of the calculated and experimental structures (vide supra) is excellent and attests to the suitability of the computational method employed herein. Furthermore, the calculated structure of $[(DAB)P]^{+}$ is consistent with those computed previously using different theoretical methods [52]. Similarly, there is good agreement between the computed metrical parameters of the models $[(DAB)As]^{+}$ and $[(DIMPY)As]^{+}$ and those reported for their corresponding crystallographically characterized analogues [21,51].

There are several noteworthy findings with regard to the structures presented in Figs. 3 and 4. Most importantly, the optimized structures of [(NACNAC)P], $[(DIMPY)P]^{+}$ and [(NACNAC)As] are not minima on the potential energy hypersurface when they are constrained to C_{2v}-symmetry. True minima are observed for these model compounds when they are optimized in C_s-symmetry; the structures thus obtained are depicted in Fig. 5 and will be discussed below. In regard to the C_{2v} structures, one important feature distinguishes the models containing DAB, DIMPY and BIPY ligands from the models including the NACNAC ligand. Whereas the relatively short Pn–N distances (P: 1.685–1.757 Å; As: 1.798–1.850 Å) in the cationic α-diimine systems that suggest the presence partial multiple-bonding, the Pn–N distances in the optimized neutral [(NACNAC)Pn] models are extremely long (P: 1.854 Å; As: 1.955 Å) and are beyond the values typically observed for single bonds. The contrast between the P–N bond distances suggests significant differences in the nature of the bonding between the ligands and the group 15 element. The contrasting behavior is highlighted by the C_s-symmetry optimized structures of [(NACNAC)Pn] which, while retaining very long Pn–N bonds, adopt boat-like conformations with a clearly pyramidal carbon environment.

Whereas the difference between the planar and non-planar [(NACNAC)Pn] structures are drastic, the planar C_s-symmetry structure of the $[(DIMPY)P]^{+}$ model is distorted only slightly away from C_{2v}-symmetry, as illustrated in Fig. 5, and the imaginary frequency corresponding to this deformation is only $-75\ cm^{-1}$. The metrical parameters of this cation suggest that it is probably best understood as being composed of an intermolecularly imine-coordinated phosphenium cation, as particularly evidenced by the dramatically different $N–C_{imine}$ bond distances of 1.320 Å and 1.291 Å and the corresponding $C_{imine}–C_{\alpha}$ distances of 1.403 Å and 1.430 Å, respectively.

To assess the structural changes that occur to the ligands upon coordination to the pnictogen centers and to evaluate the postulate that the ligands become doubly-reduced in certain instances, we have determined the optimized geometries of the free ligands (Fig. 6) and their doubly-reduced forms (Fig. 7). In both figures, only the C_{2v}-symmetry structures are presented because they are the most appropriate models for comparison to the pnictogen-containing heterocycles. It should be noted that for DAB and BIPY, the C_{2v}-symmetry structures are first-order transition states and structures and metrical parameters for the true C_{2h}-symmetry minima are presented in the Supporting information; the true minimum optimized structures of $[BIPY]^{2-}$ and $[DIMPY]^{2-}$ were not determined as these are not likely to exist as isolated dianions.

Because large changes in the angles within the ligands in their uncomplexed and complexed forms are unavoidable, the examination of such metrical parameters is not as helpful as is the comparison of bond distances. Several important observations are gleaned from the comparison of the bond distances of the ligands and those of their group 15 complexes. Perhaps the most noteworthy is that the imine-like N–C distances in the complexes involving the

Table 2
Selected computed energies for the model ligands and pnictogen complexes

Models	Symmetry[a]	N_{imag}[b]	Corrected energy[c], E_{total} (a.u.)	Relative energy (kJ mol^{-1})	HOMO (eV)	LUMO (eV)	HOMO–LUMO (eV)
Ligands							
Oxidized							
DAB	C_{2h} (1)	0	−188.0087479	0	−7.82	−2.18	5.64
	C_{2h} (2)	0	−188.0053223	8.99	−7.65	−2.42	5.23
	C_{2v}	1	−187.997689	29.04	−7.70	−2.35	5.36
$[\mathrm{NACNAC}]^-$	C_{2v}	0	−226.7216236		0.02	3.80	3.78
DIMPY	C_{2v}	0	−435.0009775		−7.32	−2.17	5.15
BIPY	C_{2h}	0	−495.1845832	0	−6.74	−1.79	4.95
	C_{2v}	1	−495.1735031	29.09	−6.78	−1.81	4.97
Reduced							
$[\mathrm{DAB}]^{2-}$	C_{2v}	0	−187.8128015		7.09	7.45	0.36
$[\mathrm{NACNAC}]^{3-}$	C_{2v}	0	−226.2856646		8.34	8.77	0.43
$[\mathrm{DIMPY}]^{2-}$	C_{2v}	2	−434.8818511		5.48	5.90	0.42
$[\mathrm{BIPY}]^{2-}$	C_{2v}	3	−495.0533583		5.16	5.74	0.58
Complexes							
P species							
$[(\mathrm{DAB})\mathrm{P}]^+$	C_{2v}	0	−529.1543655		−12.33	−7.51	4.82
[(NACNAC)P]	C_{2v}	1	−568.0027854	25.31	−3.50	−1.96	1.53
	C_s	0	−568.0124268	0	−3.95	−1.87	2.08
$[(\mathrm{DIMPY})\mathrm{P}]^+$	C_{2v}	1	−776.1639187		−10.28	−6.93	3.35
	C_s	0	−776.1638783		−10.28	−6.87	3.41
$[(\mathrm{BIPY})\mathrm{P}]^+$	C_{2v}	0	−836.3003994		−9.65	−6.30	3.36
As species							
$[(\mathrm{DAB})\mathrm{As}]^+$	C_{2v}	0	−2423.677708		−11.90	−7.56	4.35
[(NACNAC)As]	C_{2v}	1	−2462.543142	15.67	−3.55	−1.87	1.68
	C_s	0	−2462.549112	0	−3.91	−1.81	2.10
$[(\mathrm{DIMPY})\mathrm{As}]^+$	C_{2v}	0	−2670.6982		−10.01	−6.77	3.24
$[(\mathrm{BIPY})\mathrm{As}]^+$	C_{2v}	0	−2730.827911		−9.43	−6.31	3.12
Dications							
$[(\mathrm{NACNAC})\mathrm{P}]^{2+}$	C_{2v}	0	−567.362344		−19.12	−14.08	5.04
$[(\mathrm{NACNAC})\mathrm{As}]^{2+}$	C_{2v}	0	−2461.895212		−18.58	−14.03	4.55

[a] Point group symmetry.

[b] Number of imaginary vibrational frequencies.

[c] $E_{\mathrm{total}} = E_{\mathrm{calculated}} + \mathrm{ZPVE}$.

neutral ligands (DAB, DIMPY, and BIPY) are longer than those observed for the free ligands. In stark contrast, the N–C distances in the optimized [(NACNAC)Pn] complexes (for both the C_{2v} and C_s models) are almost identical to that found in the free anion $[\mathrm{NACNAC}]^-$. Similarly, while there are obvious and significant contractions of the $\mathrm{C}_{\mathrm{imine}}$–$\mathrm{C}_\alpha$ bonds for each of the complexes of the neutral ligands, there is only a slight contraction observed for the complexes of $[\mathrm{NACNAC}]^-$. Thus, once again, the metrical parameters highlights the considerably different behavior of the β-diketiminate ligand.

In regard to the metrical parameters calculated for the species containing DAB, DIMPY and BIPY ligands, it is also noteworthy that the distances observed for the $[(\mathrm{DAB})\mathrm{Pn}]^+$ models are more similar to those calculated for the doubly-reduced $[\mathrm{DAB}]^{2-}$ dianion than those for the free ligand. For the DIMPY and BIPY complexes, many of the metrical parameters appear to fall between those found in the neutral and doubly-reduced ligands, with the $[(\mathrm{DIMPY})\mathrm{Pn}]^+$ complexes having parameters closer to those of the doubly-reduced ligand than are the corresponding parameters in the $[(\mathrm{BIPY})\mathrm{Pn}]^+$ complexes. For example, while the imine $\mathrm{N{-}C}_{\mathrm{imine}}$ distance of 1.303 Å in $[(\mathrm{DIMPY})\mathrm{As}]^+$ is between the values of 1.273 Å in DIMPY and 1.331 Å in $[\mathrm{DIMPY}]^{2-}$, the $\mathrm{N{-}C}_{\mathrm{pyridyl}}$ distance of 1.385 Å in $[(\mathrm{DIMPY})\mathrm{As}]^+$ is identical to that predicted for the $[\mathrm{DIMPY}]^{2-}$ model. Overall, the examination of the metrical parameters in each of these models suggests that the DAB ligand is the most completely reduced upon complexation to a putative Pn^{I} center, followed by DIMPY and then BIPY. In sharp contrast, the bond distances in the $[\mathrm{NACNAC}]^-$ anion appear to be largely unaffected by complexation to the electron-rich group 15 center.

In order to quantify the nature of the interaction between the various ligands and the pnictogen atoms, we performed NBO population analyses of each of the model compounds and pertinent results are compiled in Tables 3 and 4. With regard to the discussion of the metrical parameters described above, it is noteworthy that the NBO Wiberg bond indices (WBI) mirror the trends suggested by the analysis of the bond distances. For example, whereas the Wiberg bond indices for the N–C bonds and

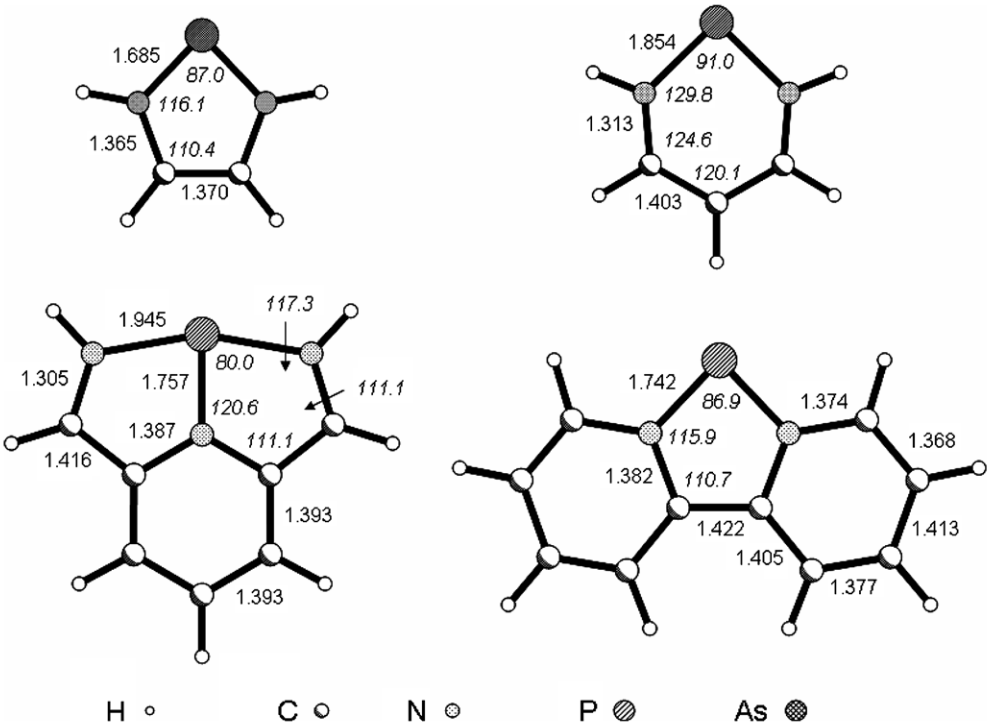

Fig. 3. Optimized structures (C_{2v}-symmetry) of the phosphorus-containing species $[(DAB)P]^+$, $[(NACNAC)P]$, $[(DIMPY)P]^+$, and $[(BIPY)P]^+$. Selected bond distances (Å) and angles (°) are indicated.

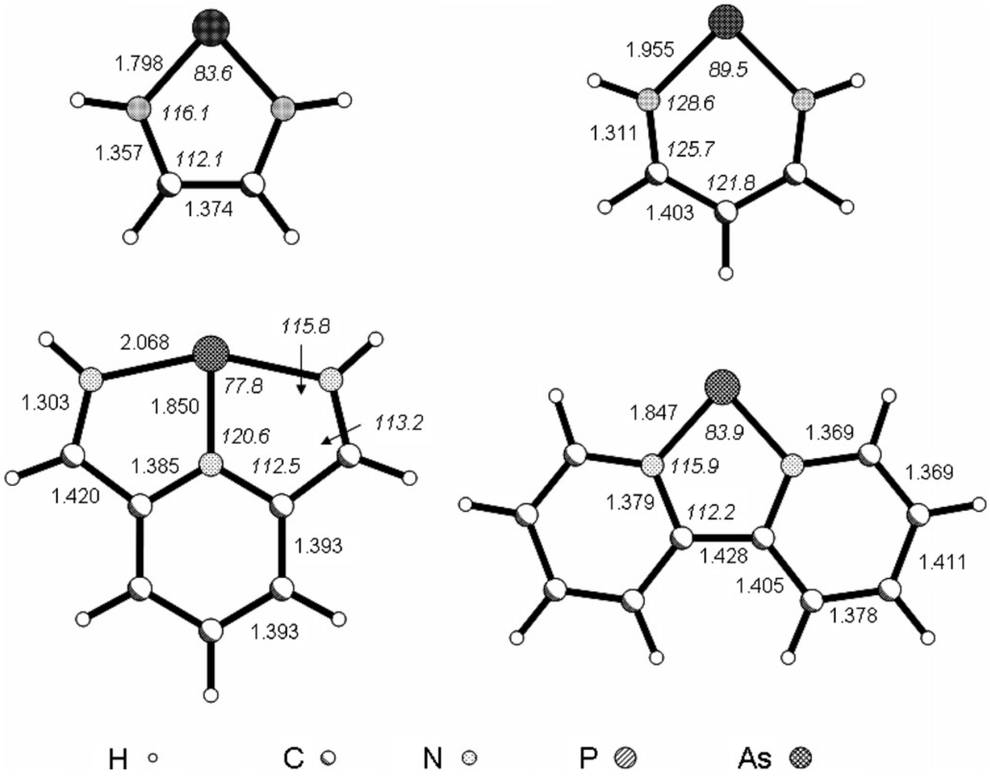

Fig. 4. Optimized structures (C_{2v}-symmetry) of the arsenic-containing species $[(DAB)As]^+$, $[(NACNAC)As]$, $[(DIMPY)As]^+$, and $[(BIPY)As]^+$. Selected bond distances (Å) and angles (°) are indicated.

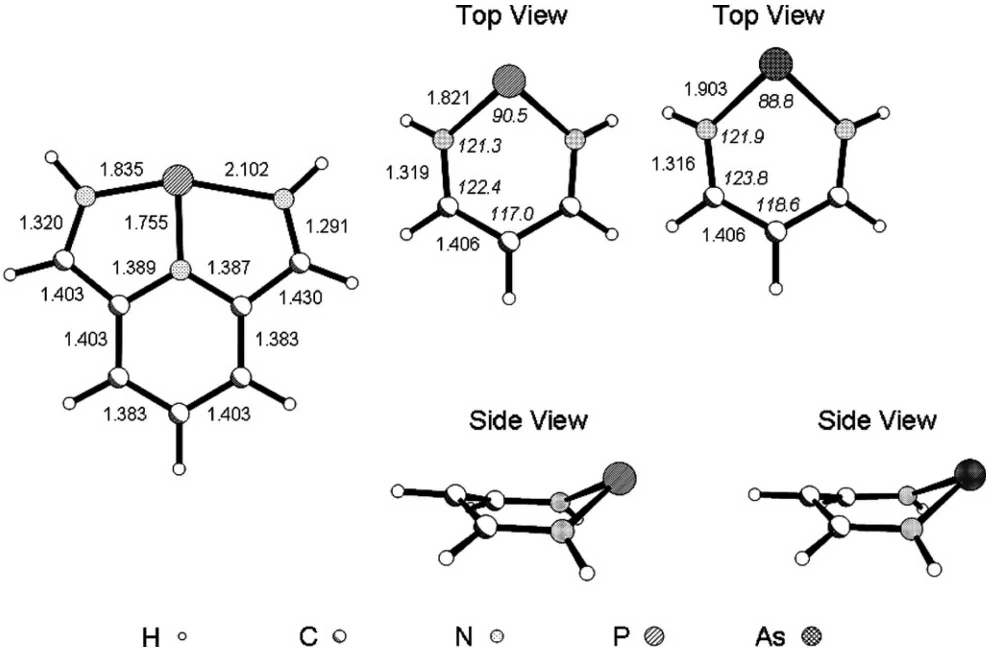

Fig. 5. Optimized structures (C_s-symmetry) of the phosphorus- and arsenic-containing species $[(DIMPY)P]^+$, [(NACNAC)P], [(NACNAC)As]. Selected bond distances (Å) and angles (°) are indicated.

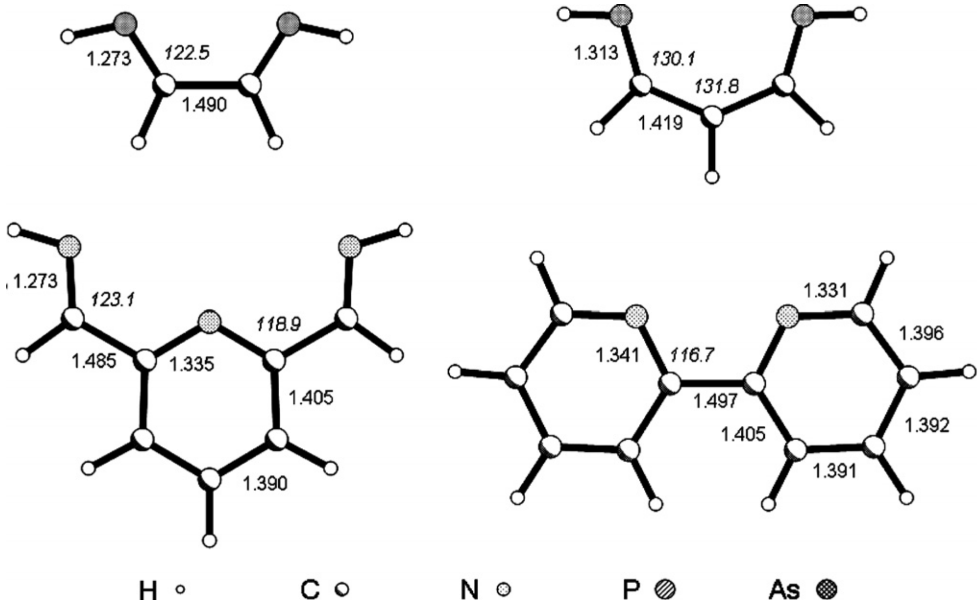

Fig. 6. Optimized structures (C_{2v}-symmetry) of the free ligands DAB, $[NACNAC]^-$, DIMPY, and BIPY. Selected bond distances (Å) and angles (°) are indicated.

the C–C bonds in $[(DAB)Pn]^+$ are almost identical to those in the $[DAB]^{2-}$ dianion, the corresponding values for the neutral [(NACNAC)Pn] models are much closer to those observed in the free $[(NACNAC)]^-$ anion. While the indices for the $[(BIPY)Pn]^+$ models fall between those of the neutral and doubly-reduced ligands, as anticipated on the basis of the metrical parameters, it is somewhat surprising that the indices for the N–C and C–C bonds in the $[(DIMPY)Pn]^+$ are remarkably similar to those in the doubly-reduced $[DIMPY]^{2-}$ dianion.

The Wiberg bond indices of the Pn–N bonds provide some initial insight into the magnitude of the interactions between the various ligand and the group 15 element. Most notably, the WBIs for the Pn–N bonds are greatest for the $[(DAB)Pn]^+$ models, which exhibit the shortest bonds between those elements. The next highest indices are observed for the bonds between the pnictogen atoms and the pyridyl nitrogen atoms in the DIMPY ligands; the values for these indices are very similar to those calculated for the $[(BIPY)Pn]^+$ models and suggest that such cations may

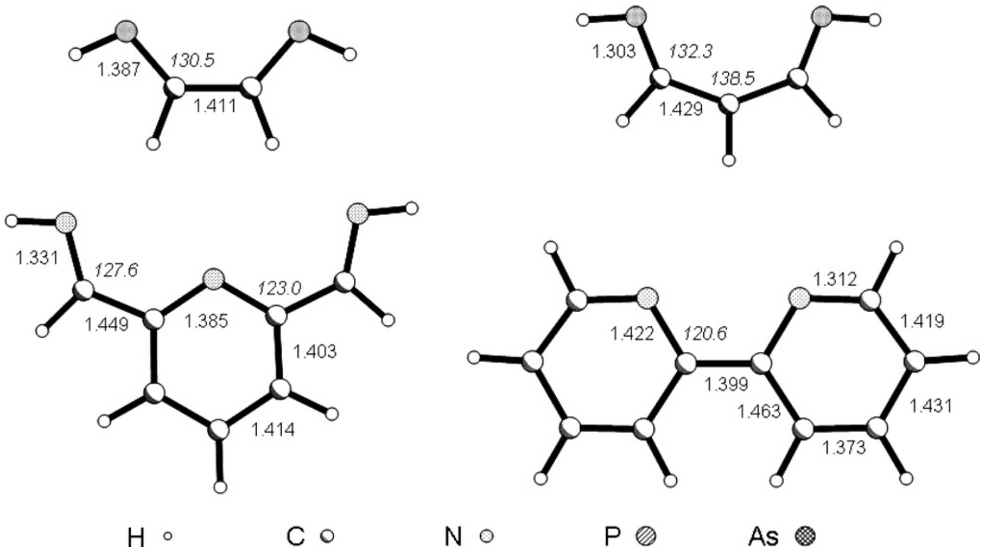

Fig. 7. Optimized structures (C_{2v}-symmetry) of the doubly-reduced ligands $[DAB]^{2-}$, $[NACNAC]^{3-}$, $[DIMPY]^{2-}$, and $[BIPY]^{2-}$. Selected bond distances (Å) and angles (°) are indicated.

Table 3
Selected computed data for the model ligands

Model	Symmetry[a]	q(N)[b]	N–C_{imine} WBI[c]	C_{imine}–C_{α} WBI[c]	π HOMO[d] (eV)	π LUMO[d] (eV)	π HOMO–LUMO (eV)
Oxidized							
DAB	C_{2h} (1)	−0.62	1.9256	1.0487	−8.19	−2.18	6.01
	C_{2h} (2)	−0.59	1.9433	1.0512	−8.97	−2.42	6.55
	C_{2v}	−0.58	1.9506	1.0276	−8.60	−2.35	6.25
$[NACNAC]^{-}$	C_{2v}	−0.81	1.6575	1.315	0.02	4.47	4.45
DIMPY	C_{2v}	−0.58 (−0.36)[e]	1.9377	1.0366	−7.37	−2.17	5.20
BIPY	C_{2h}	−0.46	1.3802	1.0402	−6.74	−1.79	4.95
	C_{2v}	−0.41	1.3863	1.0343	−6.78	−1.81	4.98
Reduced							
$[DAB]^{2-}$	C_{2v}	−1.14	1.2941	1.5346	7.09	9.51	2.42
$[NACNAC]^{3-}$	C_{2v}	−1.02	1.8007	1.339	6.74	10.82	4.08
$[DIMPY]^{2-}$	C_{2v}	−0.85 (−0.69)[e]	1.5374	1.1819	5.48	6.58	1.10
$[BIPY]^{2-}$	C_{2v}	−0.54	1.0989	1.4436	5.16	7.13	1.97

[a] Point group symmetry.
[b] NBO charge on the dicoordinate imine N atoms.
[c] NBO Wiberg bond indices for the specified bonds.
[d] Frontier orbitals involving only the π-system in the ligands.
[e] NBO charge of the $N_{pyridyl}$ atom.

be reasonable synthetic targets. The Pn–N bond indices for the [(NACNAC)Pn] models are considerably smaller than those of the cationic α-diimine models and suggest that the long P–N bonds may be considerably weaker than those in the other models.

Two other quantities obtained from the NBO analyses may provide insight into the nature of the ligand–Pn interaction and are worthy of discussion. Firstly, the almost negligible positive charges (0.24–0.3) on the Pn atoms in the [(NACNAC)Pn] models (Table 4) demonstrate that the pnictogen centers in these compounds are considerably more electron-rich than are the Pn atoms in any of the other model compounds ($q(\mathrm{Pn}) > 0.87$ in each case). Such an observation is consistent with the trends observed for the metrical parameters which suggest that the NACNAC ligand does not become reduced significantly.

More importantly in the context of intermolecular ligand reduction, the population of one of the valence p orbitals on the Pn center can be used to gauge (admittedly in a rough manner) of the amount of electron density transferred from the pnictogen to the ligand. Using the assumption for such an analysis that a singlet Pn^{I} cation suitable for ligation should have a population of 2.0 electrons in two valence orbitals and that the interaction of the ligands will generate the σ-framework of the molecule (with one of the filled valence orbitals becoming a "lone pair" of electrons), the most obvious transfer of electron density should be manifested in the population of the valence p orbital of

Table 4
Selected electron population analysis data for the model pnictogen complexes

Model	Symmetry[a]	Occupancy of Pn p(π)[b]	q(Pn)[c]	q(N)[c]	Pn–N WBI[d]	N–C_{imine} WBI[d]	C_{imine}–C_{α} WBI[d]
P species							
[(DAB)P]$^+$	C_{2v}	0.893	1.18	−0.86	1.0496	1.2281	1.5450
[(NACNAC)P]	C_{2v}	1.905	0.24	−0.79	0.6690	1.4854	1.3278
	C_s	1.408	0.27	−0.81	0.6900	1.4579	1.3489
[(DIMPY)P]$^+$	C_{2v}	1.046	0.98	−0.76	0.6129	1.5475	1.2318
				−0.62[e]	0.8738[e]		
	C_s	1.040	0.99	−0.79	0.7498	1.4377	1.2945
				−0.72	0.4560	1.6682	1.1714
				−0.62[e]	0.8786[e]		
[(BIPY)P]$^+$	C_{2v}	1.278	0.87	−0.59	0.8559	1.1486	1.2079
As species							
[(DAB)As]$^+$	C_{2v}	0.916	1.22	−0.87	0.9995	1.2614	1.5085
[(NACNAC)As]	C_{2v}	1.924	0.28	−0.80	0.6316	1.4955	1.3352
	C_s	1.473	0.30	−0.81	0.6486	1.4751	1.3472
[(DIMPY)As]$^+$	C_{2v}	1.076	1.04	−0.76	0.5624	1.5763	1.2179
				−0.62[e]	0.8411[e]		
[(BIPY)As]$^+$	C_{2v}	1.318	0.90	−0.60	0.8011	1.1649	1.3083
Dications							
[(NACNAC)P]$^{2+}$	C_{2v}	0.592	1.52	−0.86	1.0119	1.2979	1.4200
[(NACNAC)As]$^{2+}$	C_{2v}	0.565	1.61	−0.88	0.9499	1.3286	1.4131

[a] Point group symmetry.
[b] NBO population of the valence p orbital on the Pn atom of suitable symmetry to interact with the π-system of the ligand.
[c] NBO charge on the dicoordinate P atom.
[d] NBO Wiberg bond indices for the specified bonds.
[e] NBO charges and Wiberg bond indices involving the $N_{pyridyl}$ atom.

π-type symmetry (p(π)). In this light, several observations are noteworthy. Perhaps most obviously, the occupancy of the valence p(π) for both the [(DAB)Pn]$^+$ and [(DIMPY)Pn]$^+$ models are considerably lower than 2.0 (ranging from 0.893 to 1.076 electrons) and are consistent with significant transfer of electron density from the Pn atom to the ligand. While the [(BIPY)Pn]$^+$ models are consistent with somewhat less transfer of electron density (P: 1.278; As: 1.318), the magnitudes of the transferred electron density is significantly larger than those calculated for phosphine-stabilized Pn^{I} centers [13,15]. Probably the most important observation is that the occupancy of the Pn p(π) orbitals in the C_{2v}-symmetry [(NACNAC)Pn] models (P: 1.905; As: 1.924) suggest that virtually no electron density is transferred to the π-system of the ligand! The adoption of the non-planar structure reduces the occupancy of the corresponding orbitals in the C_s-symmetry [(NACNAC)Pn] models and suggest one reason for the adoption of the non-planar structure.

For phosphine-stabilized Pn^{I} cations, the transfer of electron density was considered in terms of hyperconjugation (or back-bonding) between the p(π) orbital and the ligand π-system. For the systems in this work, the greater magnitude of the donation suggests that it may be more appropriate to call the interaction Pn–ligand electron transfer in the case of the DAB ligand, however, the underlying concept is the same in both instances (it is just much more difficult to reduce a phosphine than a diimine). To understand how the ligands do or do not remove electron density from the supposed Pn^{I} cations, one must examine the shape and composition of important molecular orbitals on the ligands. MOLDEN depictions of all of the frontier orbitals for each of the ligands are supplied in the Supporting information, however, given the discussion regarding the population of the Pn p(π) orbital, the composition of the vacant orbitals involving the π-system on each free ligand are presumably the most relevant. The lowest unoccupied molecular orbitals involving the π-system are depicted in Fig. 8 and illustrate an important difference between the neutral ligands and the [NACNAC]$^-$ chelate. Whereas the LUMO in each of the neutral ligands is of the correct symmetry (B_1 in C_{2v}) to interact with a filled p(π) orbital on the Pn^{I} center, the lowest vacant orbital involving the π-system on the [NACNAC]$^-$ model does not have the appropriate symmetry (A_2 in C_{2v}) to interact in the same way. In that system, the first vacant orbital of B_1 symmetry is the LUMO + 6 orbital, which is significantly higher in energy than the LUMO (5.67 eV versus 4.47 eV) and which is based primarily on the unique α-carbon atom in the ligand.

In regard to the composition of the orbitals of the neutral ligands depicted in Fig. 8, one other point should be noted. Because of its relatively localized nature, population of the LUMO in the DAB model will have a dramatic and obvious effect on the metrical parameters of the resultant structure. In contrast the LUMOs of the BIPY and DIMPY are considerably more delocalized and thus the changes in individual bond distances in the ligands upon population of the LUMO are anticipated to be more subtle. For this reason, population analyses of the type presented herein are a valuable tool for the examination of such systems.

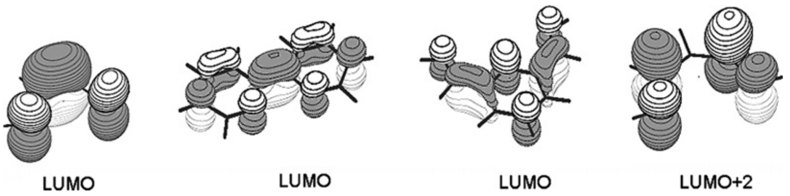

Fig. 8. Lowest unoccupied molecular orbitals involving the π-systems on the model ligands DAB, BIPY, DIMPY and $[NACNAC]^-$ in C_{2v} symmetry.

While it appears that the differing nature of the vacant orbitals explains the contrasting behavior of the neutral ligands there does not appear to be any obvious correlation between the apparent "amount" of reduction observed for the various ligands and the HOMO–LUMO energy differences (Table 2) or the energy differences between the highest occupied and lowest unoccupied orbitals of π-type symmetry (Table 3). However, it may be important to note that the overall energy of the LUMO in DAB is the lowest, followed by that of DIMPY, then BIPY and finally $[NACNAC]^-$, thus the apparent magnitude of ligand reduction may be related to that energy. This correlation also fits with the anticipated behaviors of the ligands: it should be easier to reduce the neutral four π-electron system in DAB than to reduce the conjugated aromatic systems in the DIMPY and BIPY and all of these should be much easier to reduce than the anionic ligand that already contains six electrons in its π-system.

The composition of the filled molecular orbitals on the ligands can also provide insight into the differing nature of the interaction between Pn and the neutral and anionic ligands. Whereas the HOMOs for each of the neutral ligands corresponds to "lone pair" orbitals in the σ-systems of the molecules, the HOMO for the $[NACNAC]^-$ model involves the π-system and the largest lobe is situated on the α-carbon atom (this atom also has a relatively large negative charge of −0.559), as illustrated in Fig. 9. In this light, the observed monodentate ligation to phosphorus centers through the C_α atom should not be considered surprising or unexpected. Furthermore, given that the HOMO of the $[NACNAC]^-$ ligand is of B_1 symmetry, it is more reasonably suited to donate electron density into vacant p(π) orbitals – the shape of this occupied orbital explains why this ligand is able to interact successfully through the nitrogen atoms with electron-poor centers from group 13 [53–56] and group 14 [57,58].

Finally, an examination of some of the orbitals in the pnictogen complexes provides further insight into the electronic structure of these species. Because the orbitals for both the phosphorus- and arsenic-containing models are virtually identical in every case, only those of the arsenic-containing species are presented. For example, selected frontier orbitals of $[(DAB)As]^+$ are presented in Fig. 10. The appearances of these orbitals, in particular the "lone pair" of HOMO − 2 and the π-systems in the HOMO and HOMO − 1 orbitals, are entirely consistent with those calculated previously for group 15 [52,59,60] and group 14 *N*-heterocyclic carbenoids [61,62], and the results suggest that the description of cations of the form $[(DAB)Pn]^+$ as containing Pn^{III} centers is not unreasonable.

Selected frontier orbitals of the model $[(DIMPY)As]^+$ are depicted in Fig. 11. These orbitals are particularly informative in that they show quite clearly the σ-type "lone pair" on As in HOMO − 1 and, while there is some delocalization in the HOMO, the largest lobe is obviously located on the As center and the orbital is most consistent with it being a π-type "lone pair" on As. Such "lone pairs" are exactly consistent with the orbitals found for Arduengo's "10-Pn-3" low-coordinate, hypervalent pseudo-trigonalbipyramidal systems [24]. In this light, the description of this cation as containing As^I is likely the most appropriate in spite of the transfer of some electron density from the Pn center to the ligand.

Not surprisingly, although the situation is similar to that in $[(DIMPY)As]^+$, the orbitals are somewhat more complicated for the $[(BIPY)As]^+$ system, shown in Fig. 12. Many of the orbitals are attributable to the more extensive π-system in BIPY, however, the HOMO appears to be consistent with a π-type "lone pair" on As and HOMO − 5 is clearly a σ-type "lone pair" on As. While some Pn–N π-delocalization is apparent in HOMO − 4, it is considerably less than that observed, for example, in the HOMO of $[(DAB)As]^+$. Overall, the orbitals in $[(BIPY)As]^+$ are most consistent with the presence of an As^I center in the molecule. Such an interpretation is also in keeping with the "trapped singlet carbon" analogue [(BIPY)C] reported by Weiss and co-workers [63]. It is also worthy of note that and the energy difference between the HOMO and LUMO

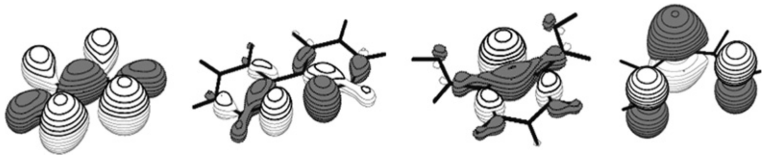

Fig. 9. Highest occupied molecular orbitals (HOMOs) for the model ligands DAB, BIPY, DIMPY and $[NACNAC]^-$ in C_{2v} symmetry.

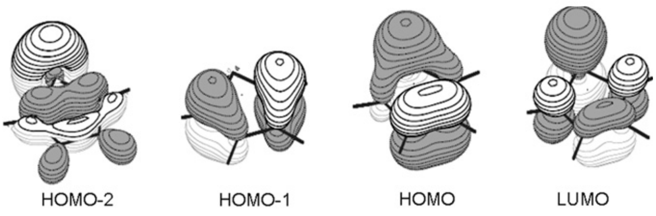

Fig. 10. Selected frontier orbitals for the model $[(DAB)As]^+$.

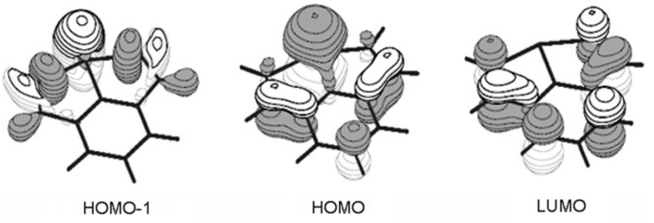

Fig. 11. Selected frontier orbitals for the model $[(DIMPY)As]^+$.

in the $[(BIPY)As]^+$ models (see Table 2) suggests that such compounds may have enough stability for their experimental isolation.

For the model [(NACNAC)As], it is instructive to examine the orbitals of both the unfavorable C_{2v} form in addition to those of the C_s form. The orbitals for the C_{2v}-symmetry compound are presented in Fig. 13. Several interesting features are observed upon examination of these orbitals. While the HOMO − 2 orbital is similar in appearance to the other σ-type "lone pair" orbitals found in the other models, the HOMO is actually quite different in detail than those of any of the complexes described above. In particular, the HOMO in [(NACNAC)As] is clearly anti-bonding in regard to the pnictogen and nitrogen atoms whereas the corresponding orbitals are either bonding (in $[(DAB)As]^+$ and $[(DIMPY)As]^+$) or non-bonding ($[(BIPY)As]^+$) in the other models. Perhaps more importantly, the HOMO − 5 also shows that the π-system in this model is not completely delocalized and; this is likely a consequence of having a non-Hückel aromatic total of eight electrons in the π-system (HOMO − 5, HOMO − 4, HOMO − 1 and HOMO are all filled). In this context, the unfavorability of the planar [(NACNAC)Pn] models is not surprising.

Distortion of the [(NACNAC)As] model from planarity to the C_s-symmetry boat conformation changes the appearances (and energies – see Table 2) of the frontier orbitals, as shown in Fig. 14. While the appearance of the σ-type "lone pair" orbitals in HOMO − 2 does not change drastically, the appearance of the HOMO is instructive. The bending of the As atom and the C_α atom toward each other allows for the in-phase overlap of the lobes on these atoms. To some extent, such overlap (and those in the other distorted orbitals) explains the dramatically lower p(π) population in the C_s-symmetry model. In any event, it must still be emphasized that the energy difference between the HOMO and LUMO are still considerably smaller for this model than for any of the other models described above and such molecules may be so reactive as to continue to elude experimental isolation.

Because the most obvious problems with the [(NACNAC)Pn] species are clearly associated with the presence of eight potential π-electrons in the six-membered ring generated by the chelation of the six π-electron $[NACNAC]^-$ fragment with the two π-electron Pn^I cation, we reasoned that the $[NACNAC]^-$ ligand would likely produce a more stable complex if it chelates to a Pn^{III} cation bearing no π-electrons. As illustrated by the data in Tables 2 and 4, the resultant dications of the form $[(NACNAC)Pn]^{2+}$ should be considerably more stable than their neutral analogues. The optimized structures for the cations are shown in Fig. 15 and the metrical parameters are clearly indicative of ligand–Pn bonding that is very different from that in [(NACNAC)Pn]. For example, the Pn–N distances in $[(NACNAC)Pn]^{2+}$ are almost identical to those in the $[(DAB)Pn]^+$ models and the N–C and C–C distances are consistent with *removal* of electron density from the HOMO of the $[NACNAC]^-$ ligand.

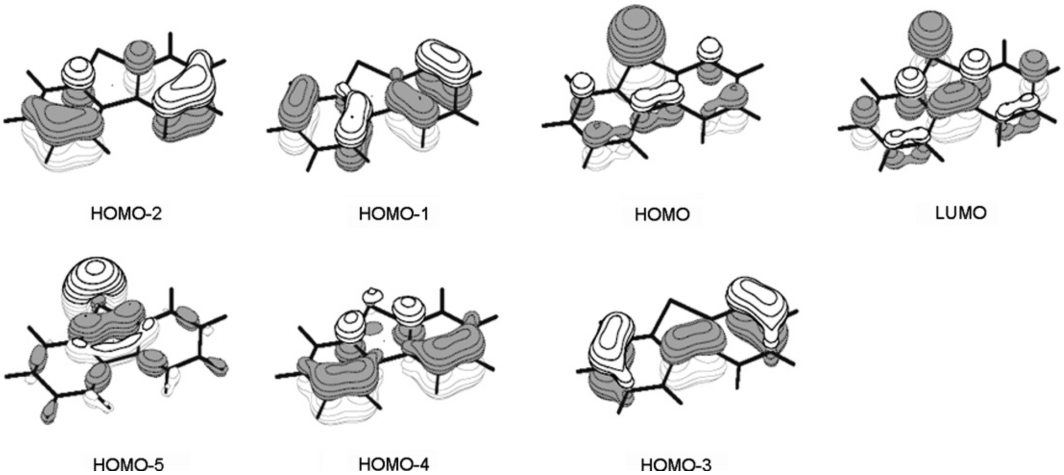

Fig. 12. Selected frontier orbitals for the model $[(BIPY)As]^+$.

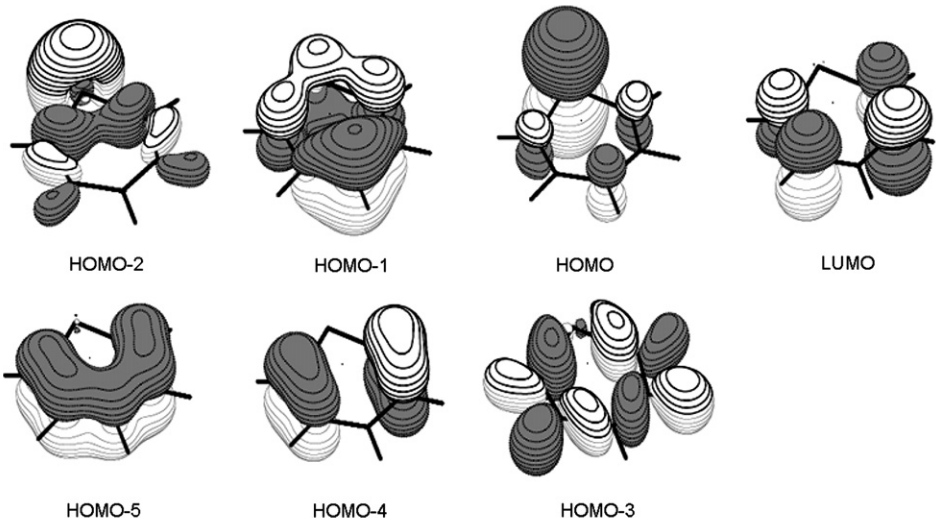

Fig. 13. Selected frontier orbitals for the C_{2v}-symmetry model [(NACNAC)As].

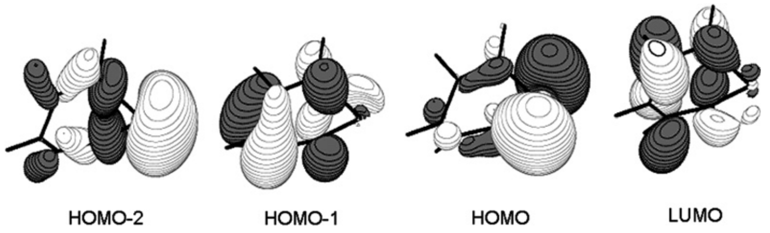

Fig. 14. Selected frontier orbitals for the C_s-symmetry model [(NACNAC)As].

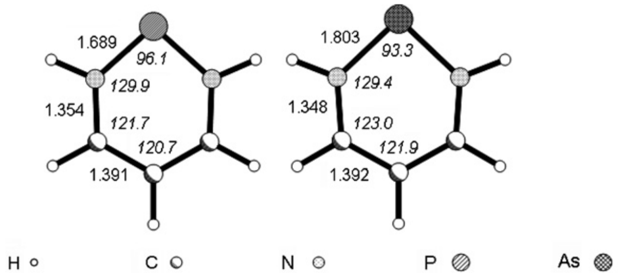

Fig. 15. Optimized structures (C_{2v}-symmetry) of $[(NACNAC)P]^{2+}$ and $[(NACNAC)As]^{2+}$. Selected bond distances (Å) and angles (°) are indicated.

In a similar vein, selected frontier orbitals for $[(NACNAC)As]^{2+}$ are depicted in Fig. 16 and these are much more similar to those of the $[(DAB)As]^{+}$ model in Fig. 10 than to those of either of the neutral models for [(NACNAC)As]. It is clear that the HOMO is bonding in terms of the Pn–N interaction, which looks very similar to that of the $[(DAB)As]^{+}$ model and, perhaps more importantly, the appearance of HOMO − 5 demonstrates that the π-system is completely delocalized in this case. The difference in HOMO and LUMO energies is quite large for these dications and the preponderance of the data suggest that salts of $[(NACNAC)Pn]^{2+}$ are viable synthetic targets that should be obtainable through judicious choice of counteranions. Cowley and co-workers' recent report of the isolation of salts of the form $[(R\text{-}NACNAC)P\text{-}Cl][SO_3CF_3]$ lend credence to these predictions because the cations in their isolated systems are the mono chloride adducts of these putative $[(R\text{-}NACNAC)P]^{2+}$ dications [47].

4. Conclusions

Experimental investigations in this work and those of other groups have demonstrated that the chelation of putative Pn^{I} centers by diimines is a viable and very clean method for the synthesis of Pn-containing heterocycles. In the case of the reaction of 1,4-diaryl-2,3-dimethyl-1,4-diazabutadiene with either PI_3 or a mixture of PCl_3 and $SnCl_2$, the products are salts of phosphenium cations, which contain P^{III} centers, as one would expect on the basis of the reported behavior of related systems. In contrast, when the analogous reactions using the similar β-diketiminate ligand are attempted, many products appear to be formed and the reactions are certainly not clean or quantitative.

The computational investigations reveal that whereas ligands containing α-diimine-like fragments (DAB, DIMPY, BIPY) are predicted to chelate effectively with Pn^{I} cations to produce planar complexes, the β-diketiminate anion $[NACNAC]^{-}$ form relatively unstable complexes which adopt boat-like conformations. The nature

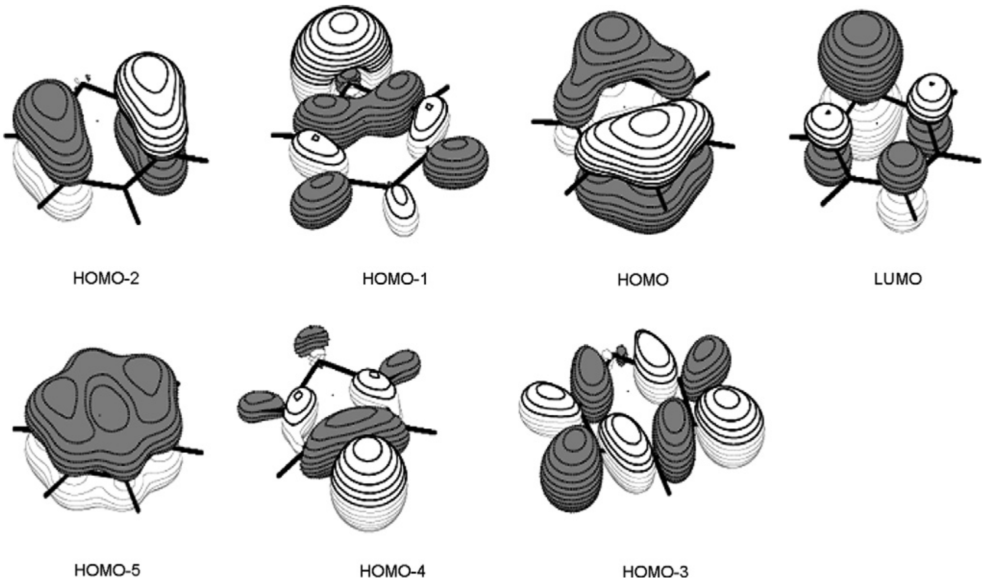

Fig. 16. Selected frontier orbitals for the C_{2v}-symmetry model $[(NACNAC)As]^{2+}$.

of the interactions between the ligands and the pnictogen atoms are also clearly dependent on the nature of the ligand and, in particular, on the symmetry and composition of the LUMO associated with the π-system on the ligands. For $[(DAB)Pn]^{+}$, the metrical parameters and population analyses are consistent with the presence of the ligand in its dianionic form and implies the oxidation of Pn^{I} to Pn^{III}. The metrical parameters for the models containing pyridyl groups, namely $[(DIMPY)Pn]^{+}$ and $[(BIPY)Pn]^{+}$ are more consistent with a smaller transfer of electron density to the ligand and can still be considered most appropriately as containing Pn^{I} centers. This conforms to the understanding that imines should be easier to reduce than pyridyl groups and suggests that many ligands containing these fragments may be employed for analogous heterocycle synthesis.

In contrast, the interaction of the six π-electron system on $[NACNAC]^{-}$ with the two π-electrons on a Pn^{I} cation produces unstable complexes and it is proposed that such anionic ligands can be more successfully employed in the stabilization of Pn^{III} centers. The large HOMO–LUMO energy difference and orbital structure consistent with known pnictogenium species suggest that the correct selection of counteranion should allow for the isolation of the dicationic $[(NACNAC)Pn]^{2+}$ salts.

Acknowledgements

We thank the Natural Science and Engineering Research Council (NSERC) of Canada for funding and scholarships (B.D.E.). We thank the Canada Foundation for Innovation, the Ontario Innovation Trust, the Ontario Research and Development Challenge Fund for support of the University of Windsor's Centre for Catalysis and Materials Research.

Appendix A. Supporting information

A summary of computational results and pictures of calculated structures and molecular orbitals are supplied. This information is available free of charge via the Internet at www.elsevier.com. CCDC 610976 and 610977 contain the supplementary crystallographic data for the structures presented in this paper. These data can be obtained free of charge from The Cambridge Crystallographic Data Centre via www.ccdc.cam.ac.uk/data_request/cif. Supplementary data associated with this article can be found, in the online version, at doi:10.1016/j.ica.2006.07.047.

References

[1] C.L.B. Macdonald, B.D. Ellis, in: R.B. King (Ed.), Encyclopedia of Inorganic Chemistry, Low Oxidation State Main Group, Wiley, Hoboken, NJ, 2005.
[2] B.D. Ellis, C.L.B. Macdonald, ACS Symp. Ser. 917 (2006) 108.
[3] F. Mathey, Angew. Chem., Int. Ed. Engl. 26 (1987) 275.
[4] K. Lammertsma, M.J.M. Vlaar, Eur. J. Org. Chem. (2002) 1127.
[5] K. Lammertsma, Top. Curr. Chem. 229 (2003) 95.
[6] A. Schmidpeter, Heteroat. Chem. 10 (1999) 529.
[7] S.F. Gamper, H. Schmidbaur, Chem. Ber. 126 (1993) 601.
[8] R.J. Barnham, R.M.K. Deng, K.B. Dillon, A.E. Goeta, J.A.K. Howard, H. Puschmann, Heteroat. Chem. 12 (2001) 501.
[9] M. Driess, H. Ackermann, J. Aust, K. Merz, C. Von Wullen, Angew. Chem., Int. Ed. 41 (2002) 450.
[10] H. Ackermann, J. Aust, M. Driess, K. Merz, C. Monse, C. Van Wullen, Phosphorus, Sulfur Silicon Relat. Elem. 177 (2002) 1613.
[11] B.D. Ellis, C.L.B. Macdonald, Phosphorus, Sulfur Silicon Relat. Elem. 179 (2004) 775.
[12] J.A. Boon, H.L. Byers, K.B. Dillon, A.E. Goeta, D.A. Longbottom, Heteroat. Chem. 11 (2000) 226.
[13] B.D. Ellis, M. Carlesimo, C.L.B. Macdonald, Chem. Commun. (2003) 1946.
[14] B.D. Ellis, C.L.B. Macdonald, Inorg. Chem. 43 (2004) 5981.
[15] B.D. Ellis, C.L.B. Macdonald, Inorg. Chem. (2006) in press.
[16] P. Kilian, A.M.Z. Slawin, J.D. Woollins, Dalton Trans. (2006) 2175.

[17] B.D. Ellis, C.A. Dyker, A. Decken, C.L.B. Macdonald, Chem. Commun. (2005) 1965.
[18] G. Reeske, C.R. Hoberg, N.J. Hill, A.H. Cowley, J. Am. Chem. Soc. 128 (2006) 2800.
[19] A.H. Cowley, R.A. Kemp, Chem. Rev. 85 (1985) 367.
[20] F. Mathey, in: M. Regitz, O.J. Scherer (Eds.), Multiple Bonds and Low Coordination in Phosphorus Chemistry, Phosphinidenes, Thieme Verlag, Stuttgart, 1990, p. 33.
[21] G. Reeske, A.H. Cowley, Chem. Commun. (2006) 1784.
[22] D. Gudat, A. Haghverdi, H. Hupfer, M. Nieger, Chem. Eur. J. 6 (2000) 3414.
[23] A.J. Arduengo III, C.A. Stewart, F. Davidson, D.A. Dixon, J.Y. Becker, S.A. Culley, M.B. Mizen, J. Am. Chem. Soc. 109 (1987) 627.
[24] A.J. Arduengo III, C.A. Stewart, Chem. Rev. 94 (1994) 1215.
[25] L. Bourget-Merle, M.F. Lappert, J.R. Severn, Chem. Rev. 102 (2002) 3031.
[26] L. Bourget-Merle, Y.X. Cheng, D.J. Doyle, P.B. Hitchcock, A.V. Khvostov, M.F. Lappert, A.V. Protchenko, X.H. Wei, ACS Symp. Ser. 917 (2006) 192.
[27] H.W. Roesky, S.S. Kumar, Chem. Commun. (2005) 4027.
[28] H.W. Roesky, ACS Symp. Ser. 917 (2006) 20.
[29] P.B. Hitchcock, M.F. Lappert, J.E. Nycz, Chem. Commun. (2003) 1142.
[30] P.J. Ragogna, N. Burford, M. D'Eon, R. McDonald, Chem. Commun. (2003) 1052.
[31] N. Burford, M. D'Eon, P.J. Ragogna, R. McDonald, M.J. Ferguson, Inorg. Chem. 43 (2004) 734.
[32] H. Tom Dieck, M. Svoboda, T. Greiser, Z. Naturforsch. B 36B (1981) 823.
[33] J. Feldman, S.J. McLain, A. Parthasarathy, W.J. Marshall, J.C. Calabrese, S.D. Arthur, Organometallics 16 (1997) 1514.
[34] A.B. Pangborn, M.A. Giardello, R.H. Grubbs, R.K. Rosen, F.J. Timmers, Organometallics 15 (1996) 1518.
[35] SMART: Molecular Analysis Research Tool, Bruker AXS Inc., Madison, WI, 2001.
[36] SAINT-Plus: Data Reduction and Correction Program, Bruker AXS Inc., Madison, WI, 2001.
[37] SADABS: An Empirical Absorption Correction Program, Bruker AXS Inc., Madison, WI, 2001.
[38] A. Altomare, M.C. Burla, M. Camalli, G. Cascarano, C. Giacovazzo, A. Guagliardi, M.A.G.G., G. Polidori, R. Spagna, SIR-97: A New Program for Solving and Refining Crystal Structures, CNR-IRMEC, Bari, 1997.
[39] G.M. Sheldrick, SHELXL-97, Universitat Göttingen, Göttingen, Germany, 1997.
[40] L.J. Farrugia, J. Appl. Crystallogr. 32 (1999) 837.
[41] G.M. Sheldrick, SHELXTL: Structure Determination Software Suite, Bruker AXS Inc., Madison, WI, 2001.
[42] M.J. Frisch, G.W. Trucks, H.B. Schlegel, G.E. Scuseria, M.A. Robb, J.R. Cheeseman, V.G. Zakrzewski, V.G. Montgomery Jr., R.E. Stratmann, J.C. Burant, S. Dapprich, J.M. Millam, A.D. Daniels, K.N. Kudin, M.C. Strain, O. Farkas, J. Tomasi, V. Barone, M. Cossi, R. Cammi, B. Mennucci, C. Pomelli, C. Adamo, S. Clifford, J. Ochterski, G.A. Petersson, P.Y. Ayala, Q. Cui, K. Morokuma, P. Salvador, J.J. Dannenberg, D.K. Malick, A.D. Rabuck, K. Raghavachari, J.B. Foresman, J. Cioslowski, J.V. Ortiz, A.G. Baboul, B.B. Stefanov, G. Liu, A. Liashenko, P. Piskorz, I. Komaromi, R. Gomperts, R.L. Martin, D.J. Fox, T. Keith, M.A. Al-Laham, C.Y. Peng, A. Nanayakkara, M. Challacombe, P.M.W. Gill, B. Johnson, W. Chen, M.W. Wong, J.L. Andres, C. Gonzalez, M. Head-Gordon, E.S. Replogle, J.A. Pople, GAUSSIAN-98, Revision A.11.1, Gaussian, Inc., Pittsburgh, PA, 2001.
[43] A.D. Becke, J. Chem. Phys. 98 (1993) 5648.
[44] J.P. Perdew, Y. Wang, Phys. Rev. B 45 (1992) 13244.
[45] A.E. Reed, L.A. Curtiss, F. Weinhold, Chem. Rev. 88 (1988) 899.
[46] G. Schaftenaar, J.H. Noordik, J. Comput.-Aided Mol. Des. 14 (2000) 123.
[47] D. Vidovic, Z. Lu, G. Reeske, J.A. Moore, A.H. Cowley, Chem. Commun. (2006) in press.
[48] F.H. Allen, Acta Crystallogr., Sect. B B58 (2002) 380.
[49] I.A. Litvinov, V.A. Naumov, T.V. Griaznova, A.N. Pudovik, A.M. Kibardin, Dokl. Akad. Nauk SSSR 312 (1990) 623.
[50] M.K. Denk, S. Gupta, A.J. Lough, Eur. J. Inorg. Chem. (1999) 41.
[51] C.J. Carmalt, V. Lomeli, B.G. McBurnett, A.H. Cowley, Chem. Commun. (1997) 2095.
[52] D. Gudat, Eur. J. Inorg. Chem. (1998) 1087.
[53] C.M. Cui, H.W. Roesky, H.G. Schmidt, M. Noltemeyer, H.J. Hao, F. Cimpoesu, Angew. Chem., Int. Ed. 39 (2000) 4274.
[54] N.J. Hardman, B.E. Eichler, P.P. Power, Chem. Commun. (2000) 1991.
[55] M.S. Hill, P.B. Hitchcock, R. Pongtavornpinyo, Dalton Trans. (2005) 273.
[56] M.S. Hill, P.B. Hitchcock, Chem. Commun. (2004) 1818.
[57] Y.Q. Ding, H.W. Roesky, M. Noltemeyer, H.G. Schmidt, P.P. Power, Organometallics 20 (2001) 1190.
[58] P.B. Hitchcock, J. Hu, M.F. Lappert, J.R. Severn, Dalton Trans. (2004) 4193.
[59] R.R. Sauers, Tetrahedron 53 (1997) 2357.
[60] R.J. Boyd, N. Burford, C.L.B. Macdonald, Organometallics 17 (1998) 4014.
[61] C. Boehme, G. Frenking, J. Am. Chem. Soc. 118 (1996) 2039.
[62] C. Heinemann, T. Mueller, Y. Apeloig, H. Schwarz, J. Am. Chem. Soc. 118 (1996) 2023.
[63] R. Weiss, S. Reichel, M. Handke, F. Hampel, Angew. Chem., Int. Ed. 37 (1998) 344.